

Mo polyoxometalate nanoparticles inhibit tumor growth and vascular endothelial growth factor induced angiogenesis

Wenjing Zheng¹, Licong Yang¹, Ying Liu¹, Xiuying Qin¹, Yanhui Zhou¹, Yunshan Zhou² and Jie Liu¹

¹Department of Chemistry, Jinan University, Guangzhou 510632, People's Republic of China

²State Key Laboratory of Chemical Resource Engineering, Institute of Science, Beijing University of Chemical Technology, Beijing 100029, People's Republic of China

E-mail: tliliu@jnu.edu.cn and zhouys@mail.buct.edu.cn

Received 17 February 2014

Accepted for publication 28 April 2014

Published 19 June 2014

Abstract


Tumor growth depends on angiogenesis, which can furnish the oxygen and nutrients that proliferate tumor cells. Thus, blocking angiogenesis can be an effective strategy to inhibit tumor growth. In this work, three typical nanoparticles based on polyoxometalates (POMs) have been prepared; we investigated their capability as antitumor and anti-angiogenesis agents. We found that Mo POM nanoparticles, especially complex **3**, inhibited the growth of human hepatocellular liver carcinoma cells (HepG2) through cellular reactive oxygen species levels' elevation and mitochondrial membrane potential damage. Complex **3** also suppressed the proliferation, migration, and tube formation of endothelial cells *in vitro* and chicken chorioallantoic membrane development *ex vivo*. Furthermore, western blot analysis of cell signaling molecules indicated that Mo POMs blocked the vascular endothelial growth factor receptor 2-mediated ERK1/2 and AKT signaling pathways in endothelial cells. Using transmission electron microscopy, we demonstrated their cellular uptake and localization within the cytoplasm of HepG2 cells. These results indicate that, owing to the extraordinary physical and chemical properties, Mo POM nanoparticles can significantly inhibit tumor growth and angiogenesis, which makes them potential drug candidates in anticancer and anti-angiogenesis therapies.

Keywords: polyoxometalates (POMs), nanoparticles, anticancer, angiogenesis, VEGF

1. Introduction

Angiogenesis, the formation of new vessels from pre-existing endothelium, is vital for reproduction, development, and repair [1]. However, excessive angiogenesis is involved with a large number of pathological processes, including growth, invasion, and metastasis in malignancies [2, 3]. Angiogenesis is tightly regulated by an intricate balance between stimulators and inhibitors [4]. Among these, the vascular endothelial growth factor (VEGF), together with fibroblast growth

factors, is a potent angiogenesis stimulator that induces vascular endothelial cell proliferation and migration [5]. VEGF exerts its biological effect mainly through the VEGF receptor 2-mediated signaling pathway [6]. VEGF receptor (VEGFR) 2 activation leads to the activation of diverse downstream signal proteins, including extracellular signal-regulated kinase (ERK) [7], phosphoinositide 3-kinase (AKT kinase) [8], focal adhesion kinase, and src family kinase [9], that promote the neovascularization in endothelial cells. This resulted in a search for new agents that target VEGF and led to an effective anti-VEGF therapy [10]. Nowadays, great progress has been made in the discovery of anti-angiogenic agents, including soluble receptors that sequester ligands [11], small molecule inhibitors that inhibit kinase activity [12], and monoclonal antibodies targeting VEGF ligands or VEGFRs [13]. Three

 Content from this work may be used under the terms of the Creative Commons Attribution 3.0 licence. Any further distribution of this work must maintain attribution to the author(s) and the title of the work, journal citation and DOI.

drugs developed for their anti-angiogenic function—bevacizumab [14], sunitinib malate, and sorafenib—have been approved to treat patients with specific types of cancer by blocking VEGF ligands or VEGFR signaling pathways [15]. However, serious side effects, such as hemorrhage, wound dehiscence, hypertensive crisis, and gastrointestinal perforation, have been associated with the currently accessible anti-VEGF agents, hindering their long-term use [15]. In addition, the inhibitors are intrinsically selective but not specific to the VEGFR, leading to treatment failure in anti-angiogenesis. Hence, there is an urgent need to discover a drug specifically targeted for the treatment of cancer that is less toxic, particularly antitumor and anti-angiogenesis agents.

As research progresses, advances in nanotechnology have become significant, leading to effective approaches for achieving efficient drugs that target tumor tissues; their efficiency is due to the extraordinary physical and chemical properties resulting from the nanosize effect. Thus, we pay special attention to an important inorganic drug candidate, polyoxometalates (POMs). POMs are early transition metal oxygen anion clusters formed by metal cations, which are bridged by oxide anions. Recently, many efforts have been made to synthesize or modify POMs by altering their structure, polarity, charge, and composition in order to obtain compounds of low toxicity, high stability, and high activity. For instance, some laboratories synthesized POMs nanoscale particles combined with $A\beta$ -targeted peptide [16] or liposome-encapsulated POMs [17]. This research is of great importance, as well as guiding significance, to the further study of POMs. As potential inorganic medical agents with antitumor, antiviral, and antibacterial activities [18], POMs are rendered attractive for applications in medicine. The histone deacetylase inhibitory activity is one of the mechanisms by which POMs exhibit their anticancer effect [19]. Moreover, POMs have also been demonstrated to interact with the basic fibroblast growth factor, potentiating itself as a typical type of inhibitor of tumor angiogenesis [20]. However, to the best of our knowledge, there are few reports showing that Mo POM nanoparticles inhibit tumor growth and VEGF-induced angiogenesis.

Over the last several years, our group systematically researched the inhibition of tumor growth and angiogenesis using the functionalized selenium nanoparticles (SeNPs) of ruthenium (II) complexes [21, 22]. However, SeNPs are very unstable and easily aggregate when there are no other surfactants or stabilizers. High cytotoxicity of ruthenium (II) complexes still exists, which is another limitation on their biocompatibility and bioefficacy. Continuing research for better inhibitors of angiogenesis, we synthesized three representative POM nanoparticles (complexes **1**, **2**, and **3**). As important inorganic drug candidates, POMs have shown promising antiviral and antitumor activities for more than a decade. With smaller size, higher stability at physiological conditions, and fewer harmful consequences, our study highlights Mo POM nanoparticles as potent anti-angiogenic agents with greatly improved nanoparticle properties and presents the possible mechanism of Mo POM nanoparticles

on the various signaling molecules involved in angiogenesis and tumor growth.

2. Experimental details

2.1. Materials and reagents

All reagents and solvents were purchased commercially and used without further purification unless specially noted. Ultrapure Milli-Q water was used in all experiments. The samples of 3-(4, 5-dimethylthiazol-2-yl)-2, 5-diphenyltetrazolium bromide (MTT) were from Sigma (St. Louis, MO, USA). The JC-1 mitochondrial membrane potential detection kit and reactive oxygen species (ROS) assay kit were from Jiancheng (Nanjing, China). Fetal bovine serum (FBS) was purchased from Gibco (Life Technologies AG, Switzerland). Dulbecco's modified Eagle's medium (DMEM) and RPMI-1640 without folic acid were from Invitrogen Corporation. The human hepatocellular liver carcinoma cell (HepG2) was purchased from the American Type Culture Collection and cultured in DMEM, supplemented with 10% FBS. Human umbilical vein endothelial cells (HUVECs) were isolated from fresh human umbilical cord veins and maintained in RPMI-1640, supplemented with 10% human serum, 10% FBS, 1% glutamin (Invitrogen), 100 IU mL⁻¹ penicillin (Sigma-Aldrich, St. Louis, MO, USA), and 100 mg mL⁻¹ streptomycin (Sigma-Aldrich). VEGF was from Chemicon (USA). Growth factor-reduced Matrigel was purchased from BD Biosciences (NJ, USA). Rabbit polyclonal antibodies against AKT, phospho-AKT, ERK1/2, and phospho-ERK1/2 were purchased from Cell Signaling Technology (Beverly, MA, USA). Anti-glyceraldehyde-3-phosphate dehydrogenase (GAPDH) was obtained from Kangchen (Shanghai, China). Horseradish peroxidase (HRP) conjugated anti-rabbit IgG was purchased from Millipore (Billerica, MA, USA). All other chemicals used were purchased from Sigma.

2.2. MTT assay

HepG2, human melanoma cells (A375), breast cancer cells (MCF-7), human low differentiation nasopharyngeal carcinoma cells (CNE-2) and HUVECs were seeded in 96-well plates at a density of 4×10^3 cells per well and exposed to various concentrations of complexes **1**, **2**, and **3**. The cells were incubated for 48 h at 37 °C, 5% CO₂, and cell viability was determined by MTT assay. Cells were treated with MTT solution (final concentration, 0.5 mg mL⁻¹) for 4 h at 37 °C in 96-well plates. The supernatants were removed carefully, which was followed by the addition of 150 μ L dimethyl sulfoxide to each well to dissolve the precipitate. The absorbance was measured at 570 nm on a microplate reader. All doses of the complexes were parallel tested in triplicate and the data were presented as averages of three independent experiments' standard deviations.

2.3. Evaluation of apoptosis levels

Apoptosis was detected with an annexin V-fluorescein isothiocyanate (FITC) kit purchased from Toyobo (Japan) according to the manufacturer's instructions. HepG2 cells were seeded in 6-well plates at a density of 1×10^5 cells per well and allowed to attach overnight. The cells were treated with complexes **1**, **2**, and **3** (5 and $10 \mu\text{g mL}^{-1}$, respectively) for 24 h, collected, and washed twice with phosphate-buffered saline (PBS). To detect early and late apoptosis, both adherent and floating cells were harvested together and re-suspended in annexin V binding buffer (10 mM HEPES/NaOH pH 7.4, 140 mM NaCl, 2.5 mM CaCl_2) at a concentration of 1×10^6 cells mL^{-1} . Subsequently, $5 \mu\text{L}$ of FITC-conjugated annexin V and $5 \mu\text{L}$ of propidium iodide were added to $100 \mu\text{L}$ of the cell suspension (1×10^5 cells). The cells were incubated for 15 min at room temperature in the dark. Finally, $400 \mu\text{L}$ of annexin V binding buffer was added to each tube and cells were analyzed by flow cytometry (FCM; BD FACSAria).

2.4. Determination of ROS

ROS levels were determined quantitatively using 2, 7-dichlorodihydrofluorescein diacetate (DCFH-DA). HepG2 cells were cultured in 6-well plates (1×10^5 cells/well) and treated with complexes **1**, **2**, and **3** (5, 10, and $20 \mu\text{g mL}^{-1}$, respectively) for 24 h. Then, both the adherent and floating cells were collected together, washed twice with PBS, and incubated with $10 \mu\text{M}$ DCFH-DA for 15 min at room temperature. Finally, the cells were analyzed by flow cytometry (FCM; BD FACSAria).

2.5. Evaluation of mitochondrial membrane potential damage

Mitochondrial membrane potential ($\Delta\Psi\text{m}$) was determined using the mitochondria-specific lipophilic cationic fluorescence dye JC-1. HepG2 cells were seeded into 6-well plates (1×10^5 cells/well) and incubated with complexes **1**, **2**, and **3** (5, 10, and $20 \mu\text{g mL}^{-1}$, respectively) for 24 h. Then, both adherent and floating cells were collected together, washed twice with PBS, and re-suspended in $300 \mu\text{L}$ JC-1 working solution in each tube. The cells were incubated for 15 min at room temperature in the dark. Finally, the cells were analyzed by flow cytometry (FCM; BD FACSAria).

2.6. Cell migration assay

HUVECs were allowed to grow into full confluence in 6-well plates pre-coated with 0.1% gelatin and then incubated with $10 \mu\text{g mL}^{-1}$ mitomycin C at 37°C , 5% CO_2 for 2 h to inactivate HUVECs. Monolayer-inactivated HUVECs were wounded by scratching with a 1 mL pipette tip. Fresh endothelial cell growth medium (ECGM) was added with three complexes in the presence or absence of VEGF, in which suramin was used as positive control. Images were taken by Nikon digital camera after 24 h and 48 h of incubation at 37°C , 5% CO_2 . The migrated cells were quantified by manual counting and percentage inhibition was expressed using

untreated wells at 100% (t test, $p < 0.05$). At least three independent experiments were performed.

2.7. Tube formation assay

Matrigel was dissolved at 4°C overnight; each well of pre-chilled 24-well plates was coated with $100 \mu\text{L}$ Matrigel and incubated at 37°C for 45 min. HUVECs (4×10^4 cells) were added in 1 mL ECGM with complexes **1**, **2**, and **3** at a dose of $10 \mu\text{g mL}^{-1}$ in the presence or absence of VEGF (20 ng mL^{-1}). After 12 h of incubation at 37°C , 5% CO_2 , endothelial cell tube formation was assessed with an inverted photomicroscope. Tubular structures were quantified by manual counting of low-power fields and inhibition percentage was expressed using untreated wells as 100%.

2.8. Chicken chorioallantoic membrane assay

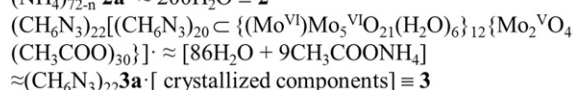
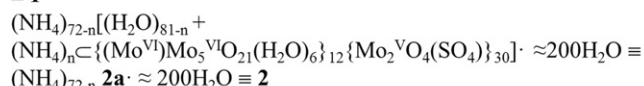
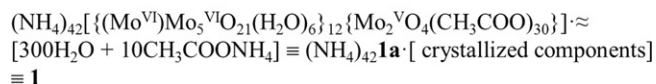
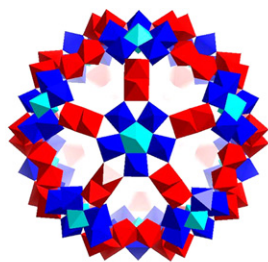
The contribution of the test complexes to angiogenesis was investigated *ex vivo* using the chick embryo chicken chorioallantoic membrane (CAM) assay. Briefly, fertilized chicken eggs (10 eggs/group) were cleaned with ethanol and incubated at 37°C and 80% humidity. On the sixth day of incubation, a square window was opened in the shell and CAMs were injected with complexes **1**, **2**, and **3** in the presence or absence of VEGF (20 ng mL^{-1}) using an insulin syringe. After 48 h of incubation, CAM arterious branches in each treatment group were photographed and counted using a Nikon digital camera system (Chiyoda-ku, Tokyo, Japan). The anti-angiogenic effect of the test complexes was presented as the relative number of arterious branches.

2.9. Assessment of nitric oxide release

Nitric oxide (NO) production was detected using a total NO assay kit from Jiancheng. HUVECs were briefly cultured in 6-well plates (1×10^5 cells/well) and treated with complexes **1**, **2**, and **3** (5, 10, and $20 \mu\text{g mL}^{-1}$, respectively) for 24 h or 48 h. The cell supernatant was then collected for NO measurement according to the manufacturer's instructions. Finally, total nitrite was quantified after the reduction of all nitrates with nitrate reductase and the effect of the complexes on the bioactivity of NO was evaluated.

2.10. Western blot analysis

HUVECs were plated into a 6-well plate (2×10^5 cells/well). After adherence, cells were incubated in serum-free medium for 24 h and then exposed to the corresponding complexes **2** and **3** for 24 h. At the end of the complexes' treatment, cells were stimulated with 20 ng mL^{-1} VEGF for 10 min at 37°C . Whole-cell lysates were collected and boiled for 10 min in $2 \times \text{SDS}$ sample buffer, subjected to 10% sodium dodecyl sulfate polyacrylamide gel electrophoresis, and transferred to nitrocellulose (Amersham Life Sciences). The blot was blocked in blocking buffer (5% nonfat dry milk/1% Tween-20 in tris-buffered saline) for 1 h at room temperature and then incubated with anti-AKT (1:1000), anti-phospho-AKT (1:500), anti-ERK1/2 (1:1000), anti-phospho-ERK1/2



Scheme 1. The basic spherical shape of the anionic clusters in complexes **1**, **2** and **3**, as well as their formulas.

(1:1000), and anti-GAPDH (1:10 000) in blocking buffer for 2 h at room temperature. The bands were then visualized using HRP-conjugated secondary antibodies (1:4000), followed by enhanced chemiluminescence (ECL; Pierce Biotech, Rockford, Illinois, USA).

2.11. Cellular uptake of complexes by transmission electron microscopy

For cellular uptake studies using transmission electron microscopy (TEM), HepG2 cells were seeded into a 6-well plate (1×10^5 cells/well) and treated with complexes **2** and **3** ($10 \mu\text{g mL}^{-1}$) for 12 h. Then, adherent cells were collected, washed twice with PBS, fixed with 3% glutaraldehyde, and stored at 4°C overnight. After centrifugation, cells were washed with PBS, fixed with 1% osmium tetroxide, dehydrated with different concentrations of ethanol, and treated overnight with acetone and embedding medium in 65°C . Finally, the sample ultra-microcut was put onto a holey carbon film on copper grids and photographed using TEM (BD Biosciences).

3. Results and discussion

Complexes **1** and **2** were synthesized according to the literature [23, 24]. Complex **3** was obtained based on complex **1** and synthesized with the method used in a previous paper [25]. The basic spherical shape of the anionic clusters in complexes **1**, **2**, and **3** and their formulas were presented in scheme 1. The anticancer and anti-angiogenesis activities of the three Mo POM nanoparticles were shown in the following strategies.

3.1. Effects of complexes on cell viability

The anti-proliferative effect of the complexes was evaluated by MTT assay in HUVECs, human hepatocellular liver

Table 1. IC_{50} values of tested complexes toward different cell lines^a.

Complexes	HUVEC	HepG2	A375	MCF-7	CNE-2
1	43 ± 2	55 ± 3	95 ± 3	>100	>100
2	24 ± 2	13 ± 3	>100	86 ± 5	>100
3	17 ± 1	9 ± 2	78 ± 3	78 ± 3	83 ± 3

^a IC_{50} values are given in $\mu\text{g mL}^{-1}$. The values are expressed as the means \pm standard deviation (triplicates).

carcinoma cells (HepG2), human melanoma cells (A375), breast cancer cells (MCF-7), and human low differentiation nasopharyngeal carcinoma cells (CNE-2). The IC_{50} values, calculated from the dose-survival curves obtained after 48 h of drug treatment, are shown in table 1. We found that IC_{50} values of complexes **1**, **2**, and **3** were 43 ± 2 , 24 ± 2 , and $17 \pm 1 \mu\text{g mL}^{-1}$ to HUVECs, while 55 ± 3 , 13 ± 3 , and $9 \pm 2 \mu\text{g mL}^{-1}$ to HepG2 cells, respectively; these were much lower than those in the other three types of cancer cells. Complex **3** showed higher cytotoxicity than complex **1** or **2**, which could be related to its better efficacy of internalizing into cells for antitumor activity. In particular, the higher cytotoxic effects of Mo POM nanoparticles on cancer cells HepG2 and normal cells HUVECs indicate that the three complexes showed a distinct preference for the HUVEC and HepG2 cells on cell proliferation.

Furthermore, HUVECs were treated with complexes **1**, **2**, and **3** for different periods of time; we found three complexes, respectively, that decreased cell survival in a time-dependent manner (figure 1(a)). HUVECs showed a good state of cell proliferation for 12 h incubation, which suggested a good action time for angiogenesis inhibition by these complexes. Next, we investigated whether complex **3** could inhibit VEGF-induced endothelial cell viability at doses ranging from 5 to $30 \mu\text{g mL}^{-1}$. As shown in figure 1(b), after a 48 h exposure to VEGF, the cell viability of HUVECs increased by nearly about 1.3-fold. And complex **3** suppressed the viability of VEGF-induced HUVECs in a concentration-dependent manner, indicating that complex **3** was a potent inhibitor for VEGF-induced endothelial cell proliferation.

3.2. Apoptosis in HepG2 cells

To quantify the cell apoptosis, HepG2 cells treated by complexes **1**, **2**, and **3** for 24 h were stained by annexin V/propidium iodide (PI). Annexin V binds to cells in early apoptosis, which can be used as a very specific apoptotic marker [26] and PI stains cells in late apoptosis and dead cells. In figure 2, the upper left square among the four squares shows cells by mechanical damage, the upper right shows late apoptotic and necrotic cells, the lower left shows normal live cells and the lower right shows early apoptosis cells. From the results, it could be detected that complex **3** ($50 + 7\%$) showed a better apoptotic effect in comparison to complex **2** ($28 + 6\%$), complex **1** ($10 + 5\%$) and the control group ($2 + 3\%$) at the concentration of $10 \mu\text{g mL}^{-1}$. Effects of complexes **1**, **2**, and **3** ($5 \mu\text{g mL}^{-1}$, respectively) on cell

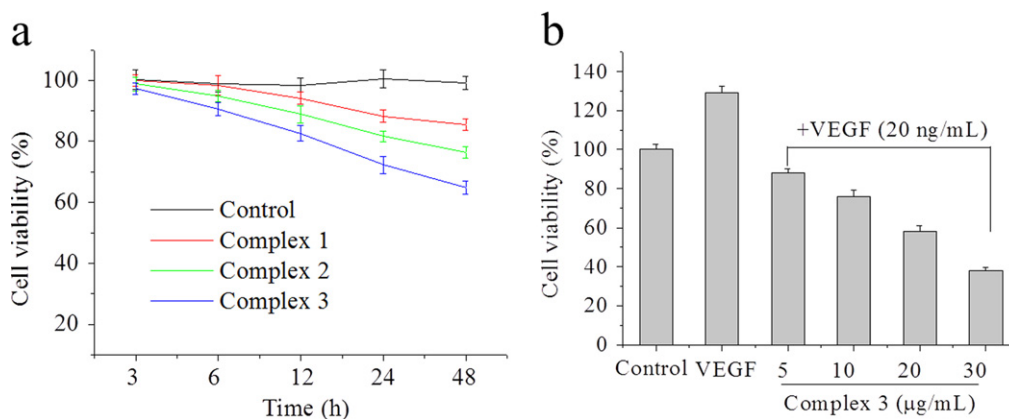


Figure 1. Effects of complexes 1, 2 and 3 on cell viability. (a) HUVECs were treated with 10 μg mL⁻¹ of complexes 1, 2, and 3 for 3, 6, 12, 24, and 48 h respectively. (b) Complex 3 inhibits VEGF-induced cell viability in HUVECs. HUVECs were treated with complex 3 from 5 to 30 μg mL⁻¹ in the presence of VEGF (20 ng mL⁻¹) for 48 h. Cell viability was determined by MTT assay. Each experiment was repeated at least three times, and the error bar stands for standard deviation (SD).

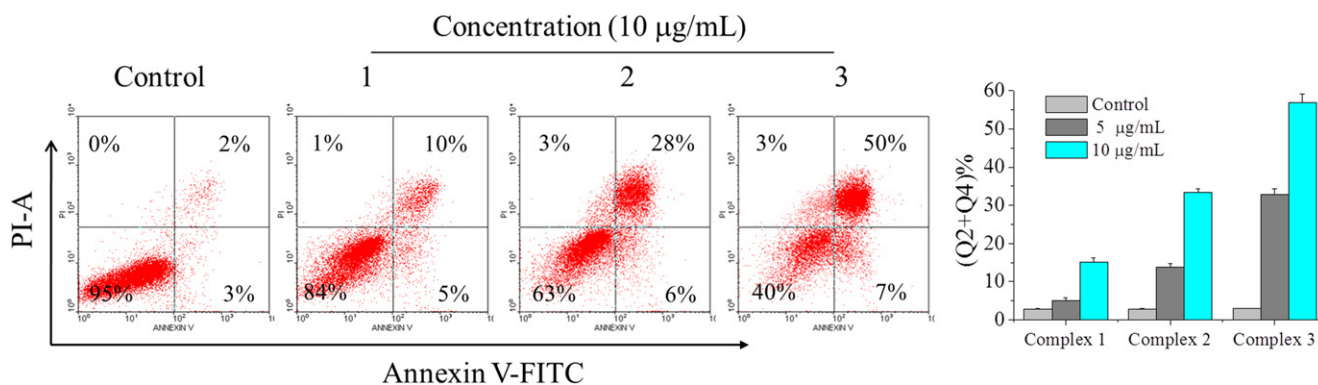


Figure 2. Effects of complexes 1, 2, and 3 on cell apoptosis. Treatment with complexes 1, 2, and 3 from 5 to 10 μg mL⁻¹ for 24 h induced apoptosis in HepG2 cells. HepG2 cells were double-stained with annexin V/PI and analyzed using flow cytometry. The experiment was performed in three independent experiments and the results are expressed as means ± SD.

apoptosis were used for further study, which showed a similar tendency. Taken together, complex 3 was more effective than complex 1 or 2 in activating apoptosis and inhibiting proliferation in HepG2 cells, which was consistent with the MTT results.

3.3. ROS levels in HepG2 cells

Reactive oxygen species production can be used as a marker of mitochondrial dysfunction and can also trigger apoptosis [27]. Additionally, ROS are mostly generated in mitochondria. Therefore, we examined the promoting effect of complexes 1, 2, and 3 on ROS generation using the fluorescent dye DCFH-DA. Figure 3 showed that ROS levels were increased to 1.1-, 2.1-, and 2.5-fold by complexes 1, 2, and 3, respectively, compared with the control group, indicating that ROS generation in HepG2 cells was elevated by these complexes. HepG2 cells treated with complexes 1, 2, and 3 at various concentrations were chosen for further study. These results demonstrated that the three complexes, especially complex 3, significantly promoted ROS production, which could mediate cells' apoptosis by mitochondrial dysfunction.

3.4. ΔΨ_m in HepG2 cells

ROS production usually precedes or accompanies the loss of ΔΨ_m. Increasing evidence has shown that mitochondrion plays an important part in the regulation of apoptosis [28]. Change in ΔΨ_m is one of the early events leading to mitochondrial functional alterations. To assess this in our cells, we used the mitochondrial probe JC-1 to measure the change of ΔΨ_m. As shown in figure 4, after exposure of HepG2 cells to complexes 1, 2, and 3 at a dose of 10 μg mL⁻¹ for 24 h, the rate of mitochondrial membrane potential dissipation increased to 4.7% (complex 1), 25.6% (complex 2), and 65.8% (complex 3), compared with the control group. HepG2 cells treated with complexes 1, 2, and 3 at various concentrations were chosen for further analysis. The results showed that the three complexes, especially complex 3, significantly attenuated the mitochondrial membrane potential, suggesting that the mitochondrial-dependent pathway may be a contributing factor in complex-induced apoptosis, which was consistent with the change in ROS levels.

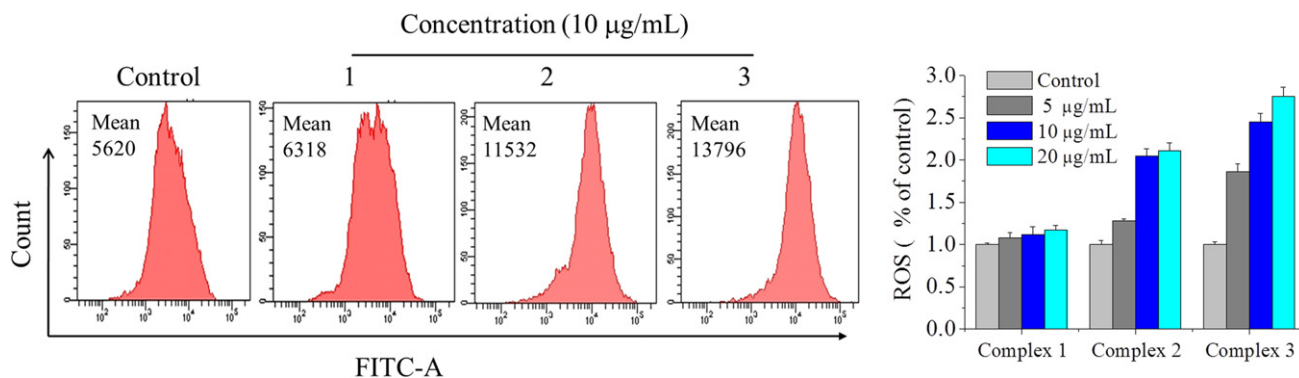


Figure 3. Effects of complexes **1**, **2**, and **3** on ROS levels in HepG2 cells. Treatment with complexes **1**, **2**, and **3** respectively from 5 to 20 $\mu\text{g mL}^{-1}$ for 24 h induced change of ROS levels in HepG2 cells. HepG2 cells were determined quantitatively using the fluorescent probe DCFH-DA and analyzed by flow cytometry. The experiment was performed in three independent experiments and the results are expressed as means \pm SD.

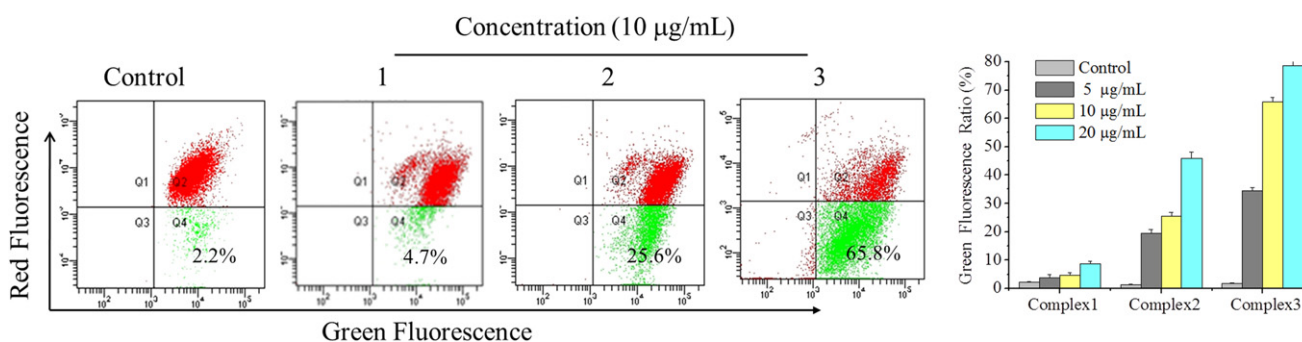


Figure 4. Effects of complexes **1**, **2**, and **3** on mitochondrial membrane potential in HepG2 cells. Treatment with complexes **1**, **2** and **3** from 5 to 20 $\mu\text{g mL}^{-1}$ for 24 h induced the change of $\Delta\Psi\text{m}$ in HepG2 cells. HepG2 cells were determined quantitatively using the fluorescent dye JC-1 and analyzed using flow cytometry. The experiment was performed in three independent experiments and the results are expressed as means \pm SD.

3.5. HUVECs migration studies

Considering the importance of angiogenesis in cancer treatment, we investigated whether the Mo POM nanoparticles would prevent angiogenesis *in vitro* assay. Cell migration is critical for endothelial cells to form blood vessels in angiogenesis and thus is necessary for tumor growth and metastasis [29]. We examined the effect of complexes **1**, **2**, and **3** with or without VEGF on the HUVECs' migration, as measured by the wound healing assay. Suramin exhibits its antitumor activity in various cell lines [30, 31], which has been clinically evaluated as a potential therapeutic in treatment of cancers caused by VEGF-induced angiogenesis; therefore, we have chosen it as a positive control. Figure 5(a) showed that for VEGF-induced angiogenesis, VEGF facilitated repair of the wounded monolayer by 24 h, and a significant area of the wound remained uncovered when treated with complexes **1**, **2**, and **3** compared to the control. The wounds treated without VEGF were wider than those in VEGF-induced migration, which could be because VEGF stimulated cell migration in the angiogenic process. Furthermore, HUVECs were treated with complexes **1**, **2**, and **3** in the presence or absence of VEGF for different periods of time and we found that the three complexes inhibited HUVECs' migration in a time-dependent manner (figures 5(b) and (c)). In particular, we

found that complex **3** could largely reduce VEGF-induced wound healing, which was superior to the suramin. Taken over, complex **3** was able to significantly block the endothelial cell migration and inhibit the angiogenesis.

3.6. HUVECs' tube formation studies

Maturation of migrated endothelial cells into a tube-like structure is a critical step for the formation of functional vessels. HUVECs were seeded onto Matrigel and stimulated to form capillary networks with VEGF (20 ng mL^{-1}). Then, the effects of complexes **1**, **2**, and **3** on HUVECs' tube formation were analyzed at the concentration of 10 $\mu\text{g mL}^{-1}$ after 12 h incubation. As shown in figure 6, robust and complete tube network formation was observed in VEGF-stimulated HUVECs compared to the non-VEGF treated group. However, this effect of VEGF was significantly inhibited by complexes **1**, **2**, and **3** and there was incomplete sprouting or branching or broken network between tubes of HUVECs. Moreover, complex **3** exhibited a stronger inhibitory effect than complex **1** or **2** in VEGF or non-VEGF-induced HUVECs' tube formation, which was even over the suramin group. Data are shown in the histogram. These results indicated the potential and significant role of complex **3** in preventing tube formation for anti-angiogenesis.

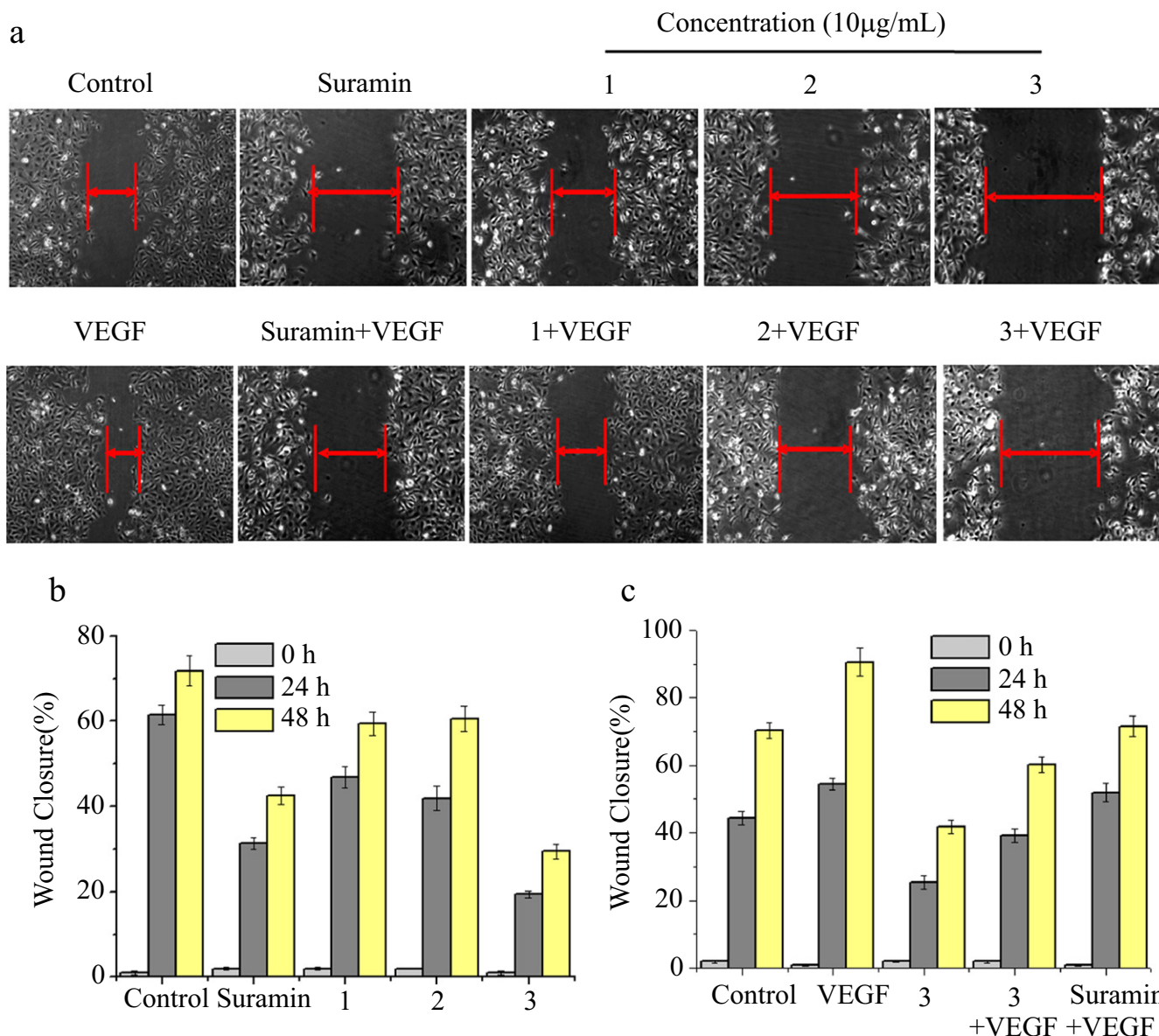


Figure 5. Effects of complexes **1**, **2**, and **3** on HUVECs' migration in wound migration assays. (a) HUVECs were treated with complexes **1**, **2**, and **3** in the presence or absence of VEGF for 24 h. (b) HUVECs were treated with complexes **1**, **2**, and **3** for 24 h and 48 h. (c) HUVECs were treated with complex **3** in the presence of VEGF for 24 h and 48 h. The concentration of VEGF is 20 ng mL⁻¹. After incubation, the migrated cells were manually counted. These experiments were performed thrice with similar results and significant differences from the control group were observed ($p < 0.05$). Data are presented as the percentages of the control group, which was set at 100%.

3.7. HUVECs' CAM assay

To confirm *in vitro* anti-angiogenic activity of complexes **2** and **3**, CAM assay was performed *ex vivo*. The fertilized chicken eggs, at day 7 of embryo development, were applied to test the anti-angiogenic effect (figure 7). We found that angiogenesis of fertilized eggs was clearly observed and new blood vessels in the VEGF-treated control were formed 1.2-fold, compared to the untreated control, after 48 h of treatment. In contrast, treatment with complexes **2** and **3** at a dose of 10 μg mL⁻¹ significantly inhibited VEGF- or non-VEGF-induced neovascularization, respectively. Data are shown in the histogram. As expected, for complex **3**, neovascular density and number were markedly more decreased on CAM

than complex **2** or suramin treated groups in the presence or absence of VEGF, indicating greater effects of complex **3** on anti-angiogenesis.

3.8. Effects of complexes on nitric oxide levels in HUVECs

Increasing evidence suggests that the PI3K/AKT/eNOS pathway is critically associated with VEGF-induced angiogenesis [32–34]. Phosphorylation-dependent activation of eNOS increases NO production, which plays an important role in VEGF-induced angiogenesis [33]. VEGF up-regulates the endothelial expression of NO synthase (NOS) and stimulates the biosynthesis of NO from cultured human umbilical venous endothelial cells [35, 36]. The nitrite content was

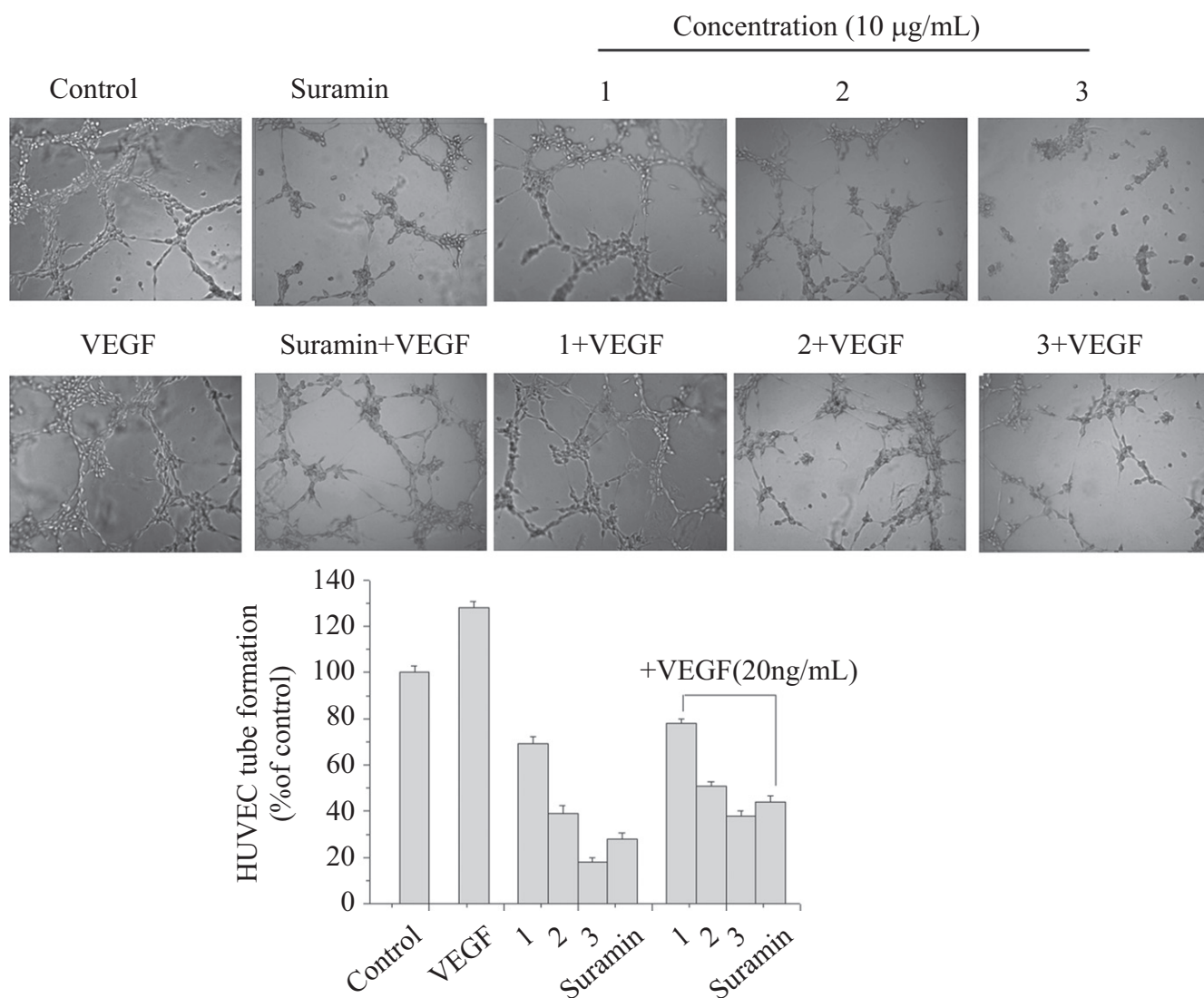


Figure 6. Effects of complexes **1**, **2**, and **3** on HUVECs' tube formation. HUVECs treated with complexes **1**, **2**, and **3** in the presence or absence of VEGF (20 ng mL⁻¹) were added onto Matrigel layers. After 12 h of incubation, HUVEC tube-like formation was assessed with an inverted photomicroscope. These experiments were performed thrice with similar results and significant differences from the control group were observed ($p < 0.05$). Data are presented as the percentages of the control group, which was set at 100%.

then measured using a total NO assay kit to determine NO generation in HUVECs. Figure 8(a) showed a significant decrease of NO level in complex-treated cells, compared to the control group, for 24 h, whereas there was no remarkable difference for another 24 h (figure 8(b)). The results suggest that the effect of complex **3** was superior to complex **1** or **2** on anti-angiogenesis and the complex-induced change in NO levels may happen at an early stage of angiogenesis. The effect of complex **3** on NO levels with or without VEGF-induced angiogenesis is shown in figure 8(c). Exposing HUVECs to only VEGF caused an increase of 37% in NO level, compared to the control group. However, a 24 h incubation of cells with complex **3** effectively inhibited the elevation of NO levels in the presence of VEGF in a concentration-dependent manner. These studies indicated that NO was a critical mediator of angiogenesis. The decrease in NO level may be because the activity of VEGF interfered

with complex **3**, further indicating that VEGF could be a potential cellular target of complexes for inhibiting angiogenesis.

3.9. ERK/AKT phosphorylation assay in HUVECs

It has been shown that phosphorylation of ERK1/2 and AKT is an important cellular signaling event for endothelial cell activation that results in the promotion of angiogenesis [33, 37]. We then determined the effects of complexes **2** and **3** on the phosphorylation of ERK1/2 and AKT in HUVECs using western blot analyses. Figure 9(a) shows that complexes **2** and **3**, especially complex **3**, caused a marked decrease in VEGF-induced phosphorylation of ERK1/2 and AKT in HUVECs when compared with the control group. As expected, the bands of P-ERK1/2 and P-AKT were increased after exposure to single VEGF. Moreover, complex **2** or **3**, in the presence of VEGF, had little effect on the total protein of

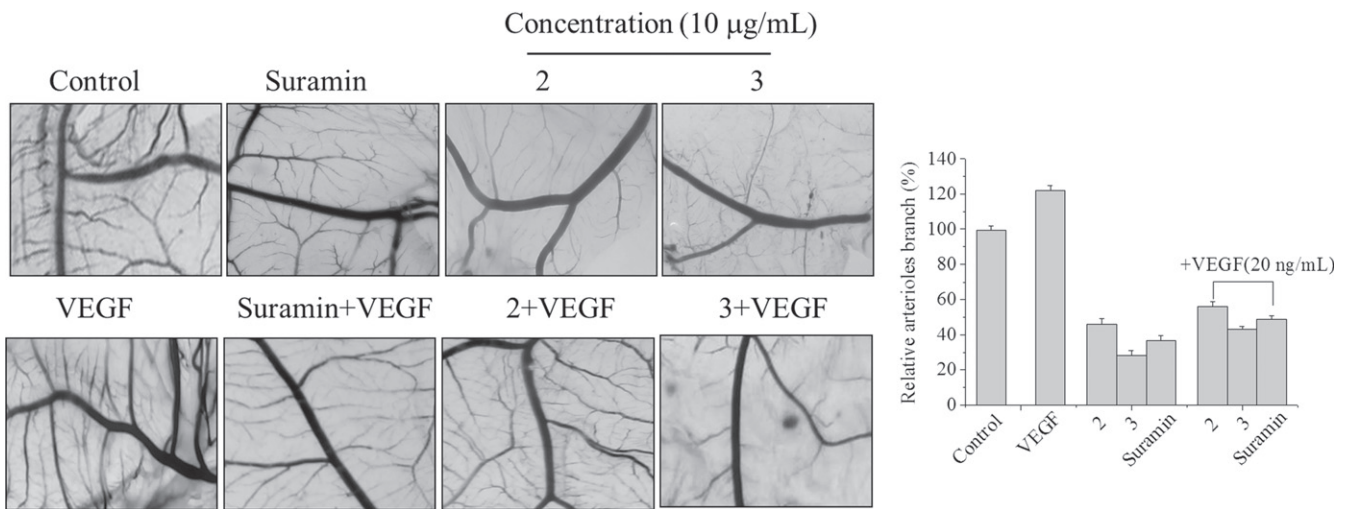


Figure 7. Angiogenic development of the arterial endpoint in the CAM inhibited by complexes **2** and **3** with or without VEGF (20 ng mL⁻¹). The various test complexes were injected into the CAM of fertilized chicken eggs on day 7 of development, and the anti-angiogenic effect of the test complexes was observed at 48 h after injection. Data are presented as the percentages of the control group, which was set at 100%.

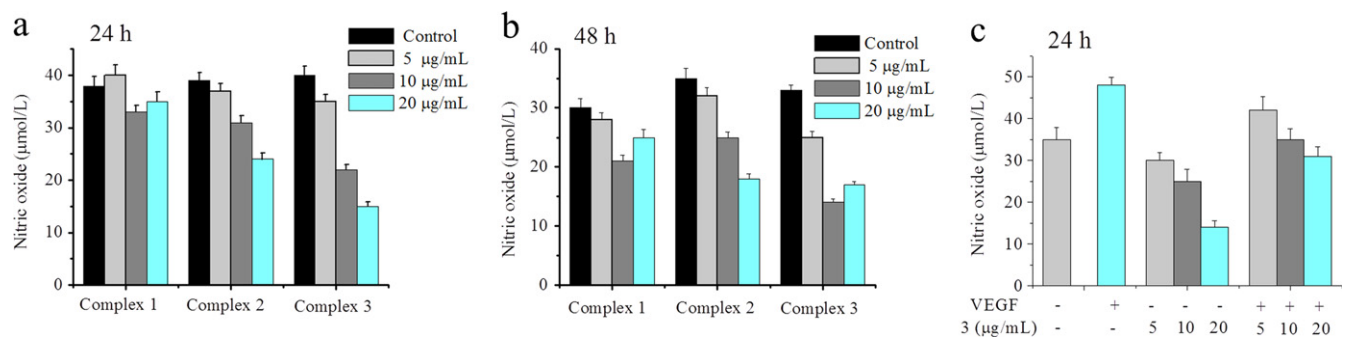


Figure 8. Effects of complexes **1**, **2**, and **3** on basal NO production. HUVECs were incubated with increasing concentrations of complexes **1**, **2**, and **3**, respectively for 24 h (a) and 48 h (b). (c) VEGF-stimulated NO production treated with complex **3** after incubating for 24 h. VEGF: 20 ng mL⁻¹. NO production was assessed spectrophotometrically by measuring its final stable equimolar degradation products, nitrite, and nitrate. The values are expressed as the means ± SD (triplicates).

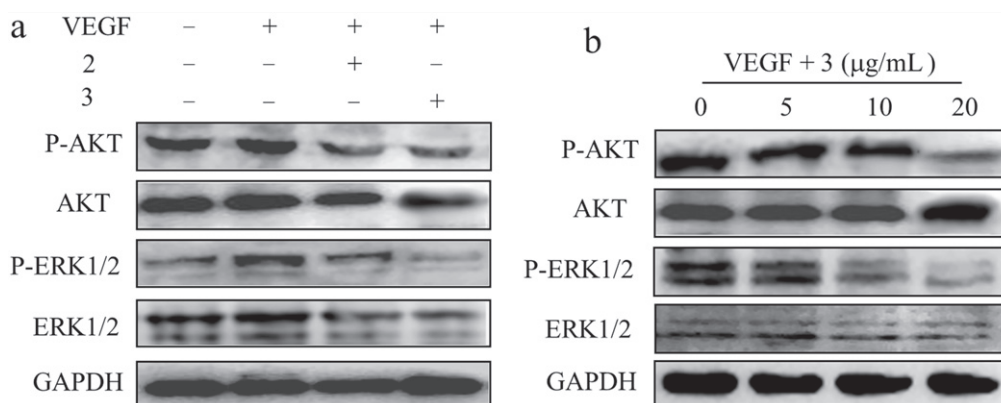


Figure 9. Effects of complexes on the intracellular signaling in HUVECs. (a) VEGF-induced phosphorylation of AKT and ERK1/2 was determined by western blotting after treatment with complexes **2** and **3** in HUVECs for 24 h. (b) Effect of complex **3** on the expression of phosphorylation of AKT and ERK1/2 in HUVECs for 24 h. GAPDH was detected as loading control. VEGF: 20 ng mL⁻¹.

ERK1/2 and AKT. We then tested the effects of complex **3** at various concentrations on the activation of VEGF-induced phosphorylation of ERK1/2 and AKT. As shown in figure 9(b), following exposure of the cells to complex **3**,

phosphorylation of ERK1/2 and AKT were significantly reduced in a dose-dependent manner after treatment for 24 h. The bands of P-ERK1/2 and P-AKT were obviously declined after exposure to complex **3** (20 μg mL⁻¹), and complex **3**

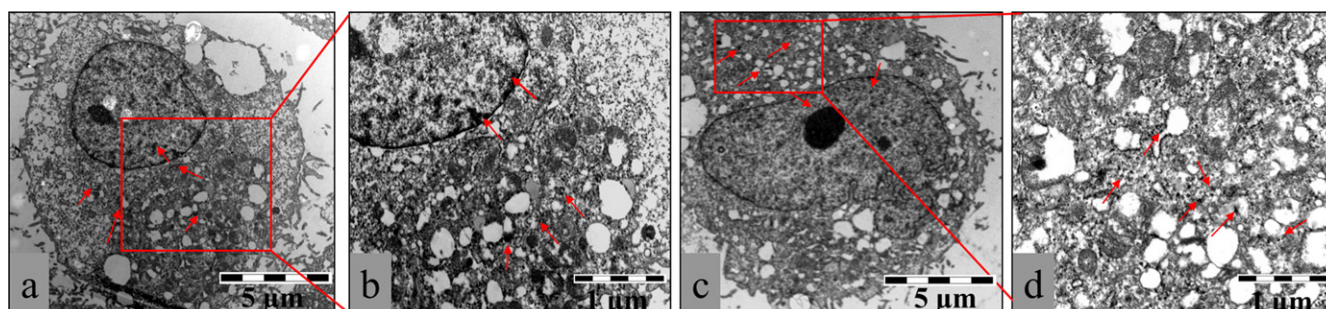


Figure 10. Representative TEM images showing the ultrastructure of HepG2 cells treated with $10 \mu\text{g mL}^{-1}$ complex **2** (a) or complex **3** (c) for 12 h. Arrows indicate complex **2** or **3**. Parts (b) and (d) are pictures with higher magnification showing detailed structures. The images are representative of three independent experiments.

treatment had no effect on the level of total ERK1/2 and AKT. These results suggest that complexes **3** and **2**, especially complex **3**, significantly inhibited the expression levels of signaling molecules' P-ERK1/2 and P-AKT proteins in the HUVECs and, in turn, inhibited proliferation and led to cell apoptosis.

3.10. Mechanisms of cellular uptake in HepG2 cells

To visualize the effects of nanoconstructs on cellular compartments, we next performed an ultra-structural analysis using TEM at the nanometer scale. Figure 10 showed that after 12 h of incubation with HepG2 cells, most of the complexes **2** and **3** were grouped in intracellular cytoplasm and only a few were clustered in perinuclear compartments and vesicular structures close to the cell nucleus. As expected, complex **3** was more evenly distributed in the cytoplasm than complex **2**, which may be because complex **3** (COOH group) had better hydrophilic property than complex **2** (SO_4^{2-} ions) and exhibited higher stability in the cytoplasm. In addition, the cell membranes were well preserved, which showed that complex **2** or **3** may be taken up by live cells via a non-endocytotic mechanism. Conversely, the highly negative surface charge of the complexes was the limit for the passive diffusion of macromolecules. Thus, we speculated that complex **2** or **3** with highly negative surface charge may be taken up into cells by active transport; this speculation still requires further study and verification.

4. Conclusions

We studied the inhibitory effects of Mo POM nanoparticles on tumor growth and angiogenesis. By determination of the cellular ROS levels' elevation and mitochondrial membrane potential dissipation, we found complex **3** had a more significant effect on inhibiting proliferation than complex **1** or **2**. Three complexes, especially complex **3**, also suppressed HUVECs' proliferation, migration, tube formation, and CAM, which were regarded as four key characteristics of endothelial cells in angiogenesis. Additionally, complex **3** could inhibit VEGF-induced angiogenesis through the largest decrease in NO levels and the expression of the signaling

molecules' P-ERK1/2 and P-AKT proteins. Using TEM, we demonstrated their cellular uptake and localization within the cytoplasm in HepG2 cells. The Mo POM nanoparticles in this study could exhibit antitumor and anti-angiogenesis effects through two distinct pathways. On one hand, three complexes could inhibit VEGF-induced angiogenesis by suppressing the AKT and ERK1/2 signaling pathways. On the other hand, a large number of nanoparticles with an extremely high negative charge may move through the cell membrane into the cytoplasm by active transport and contribute to cell apoptosis. The POM nanoparticles synthesized here also exhibited many favorable properties, including simple synthesis procedure, good water solubility, and stability under the physiological conditions. These advantages allow for further investigation of the biological activity for potential anticancer and anti-angiogenesis inhibitors.

Acknowledgments

This work was supported by the National Natural Science Foundation of China (21171070, 21371075), the Planned Item of Science and Technology of Guangdong Province (c1211220800571), the Natural Science Foundation of Guangdong Province, and the Fundamental Research Funds for the Central Universities.

References

- [1] Flier J S, Underhill L H and Folkman J 1995 *N. Engl. J. Med.* **333** 1757
- [2] Hanahan D and Folkman J 1996 *Cell* **86** 353
- [3] Angulo J, Peiró C, Romacho T, Fernández A, Cuevas B, González-Corrochano R, Giménez-Gallego G, de Tejada I S, Sánchez-Ferrer C F and Cuevas P 2011 *Eur. J. Pharmacol.* **667** 153
- [4] Hanahan D and Weinberg R A 2011 *Cell* **144** 646
- [5] Byrne A M, Bouchier-Hayes D and Harney J 2005 *J. Cell. Mol. Med.* **9** 777
- [6] Song Y, Dai F, Zhai D, Dong Y, Zhang J, Lu B, Luo J, Liu M and Yi Z 2012 *Angiogenesis* **15** 421
- [7] Chrzanowska-Wodnicka M, Kraus A. E, Gale D, White G C and VanSluys J 2008 *Blood* **111** 2647
- [8] Jiang B-H and Liu L-Z 2008 *Curr. Cancer Drug Tar.* **8** 19

- [9] Abu-Ghazaleh R, Kabir J, Jia H, Lobo M and Zachary I 2001 *Biochem. J.* **360** 255
- [10] Sitohy B, Nagy J A and Dvorak H F 2012 *Cancer Res.* **72** 1909
- [11] Holash J, Davis S, Papadopoulos N, Croll S D, Ho L, Russell M, Boland P, Leidich R, Hylton D and Burova E 2002 *Proc. Natl. Acad. Sci.* **99** 11393
- [12] Mendel D B, Schreck R E, West D C, Li G, Strawn L M, Tanciongco S S, Vasile S, Shawver L K and Cherrington J M 2000 *Clin. Cancer Res.* **6** 4848
- [13] Ferrara N 2004 *Oncologist* **9** 2
- [14] Walker E J, Su H, Shen F, Degos V, Amend G, Jun K and Young W L 2012 *Stroke* **43** 1925
- [15] Kamba T and McDonald D 2007 *Br. J. Cancer* **96** 1788
- [16] Li M, Xu C, Wu L, Ren J, Wang E and Qu X 2013 *Small* **9** 3455
- [17] Wang X, Li F, Liu S and Pope M 2005 *J. Inorg. Biochem.* **99** 452
- [18] Yamase T 2005 *J. Mater. Chem.* **15** 4773
- [19] Dong Z, Tan R, Cao J, Yang Y, Kong C, Du J, Zhu S, Zhang Y, Lu J and Huang B 2011 *Eur. J. Med. Chem.* **46** 2477
- [20] Wu Q, Wang J, Zhang L, Hong A and Ren J 2005 *Angew. Chem.* **117** 4116
- [21] Sun D, Liu Y, Yu Q, Zhou Y, Zhang R, Chen X, Hong A and Liu J 2012 *Biomaterials* **34** 171
- [22] Sun D, Liu Y, Yu Q, Qin X, Yang L, Zhou Y *et al* 2014 *Biomaterials* **35** 1572
- [23] Müller A, Zhou Y, Bögge H, Schmidtman M, Mitra T, Haupt E T and Berkle A 2006 *Angew. Chem., Int. Ed.* **45** 460
- [24] Müller A, Krickemeyer E, Bögge H, Schmidtman M and Peters F 1998 *Angew. Chem., Int. Ed.* **37** 3359
- [25] Chen Q, Yang L, Zheng C, Zheng W, Wang C, Zhang J *et al* 2014 *Nanoscale* at press doi:10.1039/C3NR05906E
- [26] Susin S A, Daugas E, Ravagnan L, Samejima K, Zamzami N, Loeffler M, Costantini P, Ferri K F, Irinopoulou T and Prévost M-C 2000 *J. Exp. Med.* **192** 571
- [27] Xia C, Meng Q, Liu L-Z, Rojanasakul Y, Wang X-R and Jiang B-H 2007 *Cancer Res.* **67** 10823
- [28] Estaquier J, Vallette F, Vayssiere J-L and Mignotte B 2012 *Advances in Mitochondrial Medicin (Advances in Experimental Medicine and Biology* vol 942) (Dordrecht: Springer) p 157
- [29] Ridley A J, Schwartz M A, Burridge K, Firtel R A, Ginsberg M H, Borisy G, Parsons J T and Horwitz A R 2003 *Science* **302** 1704
- [30] Feng Y, Li M, Wang B and Zheng Y G 2010 *J. Med. Chem.* **53** 6028
- [31] Ganesh V K, Muthuvel S K, Smith S A, Kotwal G J and Murthy K H 2005 *Biochemistry* **44** 10757
- [32] Ferrara N 2002 *Nat. Rev. Cancer* **2** 795
- [33] Lee S-J, Namkoong S, Kim Y-M, Kim C-K, Lee H, Ha K-S, Chung H-T, Kwon Y-G and Kim Y-M 2006 *Am. J. Physiol. Heart Circ. Physiol.* **291** H2836
- [34] Zachary I 2003 *Biochem. Soc. Trans.* **31** 1171
- [35] Hood J D, Meininger C J, Ziche M and Granger H J 1998 *Am. J. Physiol. Heart Circ. Physiol.* **274** H1054
- [36] van der Zee R, Murohara T, Luo Z, Zollmann F, Passeri J, Lekutat C and Isner J M 1997 *Circulation* **95** 1030
- [37] Dong G, Chen Z, Li Z-Y, Yeh N T, Bancroft C C and Van Waes C 2001 *Cancer Res.* **61** 5911